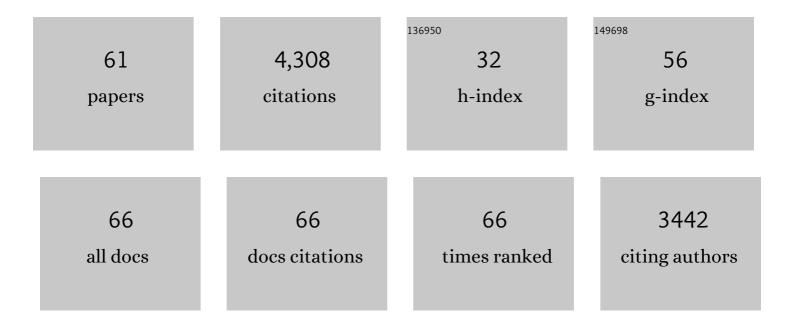
## Marie-Pierre Doin

List of Publications by Year in descending order

Source: https://exaly.com/author-pdf/6963143/publications.pdf Version: 2024-02-01



| #  | Article   | IF  | CITATIONS |
|----|---|-----|-----------|
| 1  | Numerical simulations of subduction zones. Physics of the Earth and Planetary Interiors, 2005, 149, 133-153.  | 1.9 | 427       |
| 2  | Corrections of stratified tropospheric delays in SAR interferometry: Validation with global atmospheric models. Journal of Applied Geophysics, 2009, 69, 35-50.   | 2.1 | 314       |
| 3  | Systematic InSAR tropospheric phase delay corrections from global meteorological reanalysis data.<br>Geophysical Research Letters, 2011, 38, n/a-n/a.   | 4.0 | 269       |
| 4  | A comparison of methods for the modeling of thermochemical convection. Journal of Geophysical Research, 1997, 102, 22477-22495.   | 3.3 | 239       |
| 5  | Improving InSAR geodesy using Global Atmospheric Models. Journal of Geophysical Research: Solid<br>Earth, 2014, 119, 2324-2341.   | 3.4 | 220       |
| 6  | Time series analysis of Mexico City subsidence constrained by radar interferometry. Journal of Applied<br>Geophysics, 2009, 69, 1-15.   | 2.1 | 194       |
| 7  | Mantle convection and stability of depleted and undepleted continental lithosphere. Journal of<br>Geophysical Research, 1997, 102, 2771-2787.   | 3.3 | 176       |
| 8  | Measurement of interseismic strain across the Haiyuan fault (Gansu, China), by InSAR. Earth and<br>Planetary Science Letters, 2008, 275, 246-257.   | 4.4 | 163       |
| 9  | Ground motion measurement in the Lake Mead area, Nevada, by differential synthetic aperture radar<br>interferometry time series analysis: Probing the lithosphere rheological structure. Journal of<br>Geophysical Research, 2007, 112, . | 3.3 | 154       |
| 10 | Shallow creep on the Haiyuan Fault (Gansu, China) revealed by SAR Interferometry. Journal of<br>Geophysical Research, 2012, 117, .  | 3.3 | 152       |
| 11 | Long-term growth of the Himalaya inferred from interseismic InSAR measurement. Geology, 2012, 40, 1059-1062.  | 4.4 | 136       |
| 12 | Heat transport in stagnant lid convection with temperature- and pressure-dependent Newtonian or non-Newtonian rheology. Journal of Geophysical Research, 1999, 104, 12759-12777.  | 3.3 | 129       |
| 13 | Largeâ€scale InSAR monitoring of permafrost freezeâ€thaw cycles on the Tibetan Plateau. Geophysical<br>Research Letters, 2017, 44, 901-909.   | 4.0 | 113       |
| 14 | Spatio-temporal evolution of aseismic slip along the Haiyuan fault, China: Implications for fault frictional properties. Earth and Planetary Science Letters, 2013, 377-378, 23-33.   | 4.4 | 110       |
| 15 | New Radar Interferometric Time Series Analysis Toolbox Released. Eos, 2013, 94, 69-70.  | 0.1 | 106       |
| 16 | Mexico City Subsidence Measured by InSAR Time Series: Joint Analysis Using PS and SBAS Approaches.<br>IEEE Journal of Selected Topics in Applied Earth Observations and Remote Sensing, 2012, 5, 1312-1326.                               | 4.9 | 96        |
| 17 | Subduction initiation and continental crust recycling: the roles of rheology and eclogitization.<br>Tectonophysics, 2001, 342, 163-191.   | 2.2 | 87        |
| 18 | Numerical simulations of the mantle lithosphere delamination. Journal of Geophysical Research, 2004, 109, .   | 3.3 | 86        |

MARIE-PIERRE DOIN

| #  | Article   | IF   | CITATIONS |
|----|---|------|-----------|
| 19 | Geoid anomalies and the structure of continental and oceanic lithospheres. Journal of Geophysical<br>Research, 1996, 101, 16119-16135.  | 3.3  | 76        |
| 20 | Slab surface temperature in subduction zones: Influence of the interplate decoupling depth and upper plate thinning processes. Earth and Planetary Science Letters, 2007, 255, 324-338.   | 4.4  | 69        |
| 21 | Unsupervised Spatiotemporal Mining of Satellite Image Time Series Using Grouped Frequent Sequential<br>Patterns. IEEE Transactions on Geoscience and Remote Sensing, 2011, 49, 1417-1430.   | 6.3  | 66        |
| 22 | Inversion of deformation fields time-series from optical images, and application to the long term<br>kinematics of slow-moving landslides in Peru. Remote Sensing of Environment, 2018, 210, 144-158.   | 11.0 | 65        |
| 23 | Along-strike variations of the partitioning of convergence across the Haiyuan fault system detected by InSAR. Geophysical Journal International, 2016, 205, 536-547.  | 2.4  | 61        |
| 24 | Convective destabilization of a thickened continental lithosphere. Earth and Planetary Science<br>Letters, 2002, 202, 303-320.  | 4.4  | 60        |
| 25 | Overriding plate thinning in subduction zones: Localized convection induced by slab dehydration.<br>Geochemistry, Geophysics, Geosystems, 2006, 7, n/a-n/a.   | 2.5  | 58        |
| 26 | InSAR measurement of the deformation around Siling Co Lake: Inferences on the lower crust viscosity<br>in central Tibet. Journal of Geophysical Research: Solid Earth, 2015, 120, 5290-5310.  | 3.4  | 55        |
| 27 | Numerical simulations of the cooling of an oceanic lithosphere above a convective mantle. Physics of the Earth and Planetary Interiors, 2001, 125, 45-64.   | 1.9  | 52        |
| 28 | Backâ€arc strain in subduction zones: Statistical observations versus numerical modeling.<br>Geochemistry, Geophysics, Geosystems, 2008, 9, .   | 2.5  | 52        |
| 29 | Ice loss in the Northeastern Tibetan Plateau permafrost as seen by 16 yr of ESA SAR missions. Earth and<br>Planetary Science Letters, 2020, 545, 116404.  | 4.4  | 45        |
| 30 | Strain Partitioning and Presentâ€Day Fault Kinematics in NW Tibet From Envisat SAR Interferometry.<br>Journal of Geophysical Research: Solid Earth, 2018, 123, 2462-2483.   | 3.4  | 44        |
| 31 | Transient rift opening in response to multiple dike injections in the Manda Hararo rift (Afar, Ethiopia)<br>imaged by timeâ€dependent elastic inversion of interferometric synthetic aperture radar data. Journal<br>of Geophysical Research, 2010, 115, .            | 3.3  | 34        |
| 32 | Flattening of the oceanic topography and geoid: thermal versus dynamic origin. Geophysical Journal<br>International, 2000, 143, 582-594.  | 2.4  | 33        |
| 33 | Rising of the lowest place on Earth due to Dead Sea waterâ€level drop: Evidence from SAR<br>interferometry and GPS. Journal of Geophysical Research, 2012, 117, .   | 3.3  | 31        |
| 34 | DEM Corrections Before Unwrapping in a Small Baseline Strategy for InSAR Time Series Analysis. IEEE<br>Geoscience and Remote Sensing Letters, 2014, 11, 696-700.  | 3.1  | 31        |
| 35 | Independent Component Analysis and Parametric Approach for Source Separation in InSAR Time Series<br>at Regional Scale: Application to the 2017–2018 Slow Slip Event in Guerrero (Mexico). Journal of<br>Geophysical Research: Solid Earth, 2020, 125, e2019JB018187. | 3.4  | 31        |
| 36 | Constraining the kinematics of metropolitan Los Angeles faults with a slipâ€partitioning model.<br>Geophysical Research Letters, 2016, 43, 11192-11201.   | 4.0  | 29        |

MARIE-PIERRE DOIN

| #  | Article  | IF   | CITATIONS |
|----|--|------|-----------|
| 37 | Plume-lithosphere interaction beneath a fast moving plate. Geophysical Research Letters, 2006, 33, n/a-n/a.  | 4.0  | 28        |
| 38 | From a mountain belt collapse to a sedimentary basin development: 2-D thermal model based on inversion of stratigraphic data in the Paris Basin. Tectonophysics, 2004, 386, 1-27.                                | 2.2  | 25        |
| 39 | InSAR observations of lake loading at Yangzhuoyong Lake, Tibet: Constraints on crustal elasticity.<br>Earth and Planetary Science Letters, 2016, 449, 240-245.   | 4.4  | 17        |
| 40 | 3D GNSS Velocity Field Sheds Light on the Deformation Mechanisms in Europe: Effects of the Vertical Crustal Motion on the Distribution of Seismicity. Journal of Geophysical Research: Solid Earth, 2022, 127, . | 3.4  | 16        |
| 41 | Three-dimensional numerical simulations of mantle flow beneath mid-ocean ridges. Journal of<br>Geophysical Research, 2005, 110, .  | 3.3  | 15        |
| 42 | Onset of small-scale instabilities at the base of the lithosphere: scaling laws and role of pre-existing lithospheric structures. Geophysical Journal International, 2004, 160, 345-357.                         | 2.4  | 14        |
| 43 | Influence of the precollisional stage on subduction dynamics and the buried crust thermal state:<br>Insights from numerical simulations. Tectonophysics, 2007, 441, 27-45.                                       | 2.2  | 14        |
| 44 | Interseismic deformation of the Shahroud fault system (NE Iran) from spaceâ€borne radar<br>interferometry measurements. Geophysical Research Letters, 2015, 42, 5753-5761.                                       | 4.0  | 13        |
| 45 | Localized Afterslip at Geometrical Complexities Revealed by InSAR After the 2016 Central Italy Seismic Sequence. Journal of Geophysical Research: Solid Earth, 2020, 125, e2019JB019065.                         | 3.4  | 13        |
| 46 | Terrain deformation measurements from optical satellite imagery: The MPIC-OPT processing services for geohazards monitoring. Remote Sensing of Environment, 2022, 274, 112949.                                   | 11.0 | 13        |
| 47 | FLATSIM: The ForM@Ter LArge-Scale Multi-Temporal Sentinel-1 InterferoMetry Service. Remote Sensing, 2021, 13, 3734.  | 4.0  | 11        |
| 48 | Landslides induced by the 2017 Mw7.3 Sarpol Zahab earthquake (Iran). Landslides, 2022, 19, 603-619.  | 5.4  | 10        |
| 49 | Interseismic coupling along the Mexican subduction zone seen by InSAR and GNSS. Earth and Planetary Science Letters, 2022, 586, 117534.  | 4.4  | 9         |
| 50 | The variety of subaerial active salt deformations in the Kuqa fold-thrust belt (China) constrained by<br>InSAR. Earth and Planetary Science Letters, 2016, 450, 83-95.   | 4.4  | 8         |
| 51 | Sparsity Optimization Method for Slow-Moving Landslides Detection in Satellite Image Time-Series. IEEE Transactions on Geoscience and Remote Sensing, 2019, 57, 2133-2144.                                       | 6.3  | 8         |
| 52 | A Simple Phase Unwrapping Errors Correction Algorithm Based on Phase Closure Analysis. , 2018, , .   |      | 5         |
| 53 | On the interpretation of linear relationships between seafloor subsidence rate and the height of the ridge. Geophysical Journal International, 2001, 146, 691-698.   | 2.4  | 4         |
| 54 | What can be learned from underdetermined geodetic slip inversions: the Parkfield GPS network example. Geophysical Journal International, 2013, 194, 1900-1908.   | 2.4  | 4         |

| #  | Article  | IF  | CITATIONS |
|----|--|-----|-----------|
| 55 | Ranking evolution maps for Satellite Image Time Series exploration: application to crustal<br>deformation and environmental monitoring. Data Mining and Knowledge Discovery, 2019, 33, 131-167.  | 3.7 | 4         |
| 56 | Correction to "Transient rift opening in response to multiple dike injections in the Manda Hararo rift<br>(Afar, Ethiopia) imaged by time-dependent elastic inversion of interferometric synthetic aperture radar<br>data― Journal of Geophysical Research, 2010, 115, . | 3.3 | 3         |
| 57 | Extraction of frequent grouped sequential patterns from Satellite Image Time Series. , 2010, , .   |     | 2         |
| 58 | Spatiotemporal mining of ENVISAT SAR interferogram time series over the Haiyuan fault in China. , 2011, , .  |     | 2         |
| 59 | Terrain Deformation Measurements from Optical Satellite Imagery: On-Line Processing Services for Geohazards Monitoring. , 2021, , .  |     | 2         |
| 60 | Unrest at Cayambe Volcano revealed by SAR imagery and seismic activity after the Pedernales<br>subduction earthquake, Ecuador (2016). Journal of Volcanology and Geothermal Research, 2022, 428,<br>107577.  | 2.1 | 2         |
| 61 | Iterative summarization of satellite image time series. , 2014, , .  |     | 1         |